JOURNAL OF CATALYSIS 33, 233–248 (1974)

The Limitation of the Transmission Electron Microscope for Characterization of Supported Metal Catalysts

PETER C. FLYNN AND SIEGHARD E. WANKE*

Department of Chemical Engineering, University of Alberta, Edmonton, Alberta, Canada

AND

PETER S. TURNER

Department of Physics, University of Alberta, Edmonton, Alberta

Received September 12, 1973

The accuracy of particle size distributions determined from electron micrographs is examined from both theoretical and experimental points of view. Particle detectability and apparent size are found to be sensitive functions of defocus, and hence of elevation of particles in the specimen. Contrast is shown to vary with orientation of both particles and support material. Sources of contrast inherent in the support in the subnanometer range are illustrated. It is concluded that particle size distributions become increasingly subject to error as the fraction of particles with sizes below about 2.5 nm increases.

INTRODUCTION

In the last fifteen years the electron microscope has found increasingly widespread application for the characterization of supported metal catalysts (*1–7*). A principle aim in such studies is the determination of the metal dispersion (the ratio of surface to total metal atoms) which can be calculated if the metal particle size distribution is known, and if a particle geometry is assumed. Electron microscopy has been used to provide direct determination of the size distribution from the images of the metal particles.

The claimed resolution in images of supported metal catalysts has gradually increased, to the point where the detection of 0.4 nm particles and calculated average particle sizes of less than 2 nm have been reported (*3, 6, 7*). Such particle size distributions obtained by electron microscopy are based on three implicit assumptions, namely:

a. the size of a metal particle is equal to the size of its image recorded on the micrograph (corrected for magnification);
b. detection of a particle of a given size implies that all particles of that size and all larger particles are being detected;
c. image contrast of the metal particles is distinguishable from contrast arising from the support material.

These assumptions are consistent with the use of a simple mass-thickness interpretation of image contrast in the electron microscope.

It is clear that the correctness of these assumptions is important, since particle size distributions determined from micrographs have often been used to confirm a proposed adsorption stoichiometry for the selective adsorption of gases on supported catalysts

* To whom inquiries concerning this paper should be addressed.

Copyright © 1974 by Academic Press, Inc.
All rights of reproduction in any form reserved.

(*3*, *6*). This latter technique, thus calibrated, has been used for routine determination of metal dispersions.

Recent work on the bright field imaging of atoms and atomic clusters using conventional high resolution instruments (*8*–*10*) has emphasized the importance of careful image interpretation, using theories which take into account the defects of the imaging lens (*11*). On the basis of such results and of the characteristics of the specimens involved, we suspected that none of the above assumptions was necessarily valid, particularly for smaller metal particles, and that limits should be determined for both the smallest reliable particle size and the smallest reliable difference between the size of two particles.

In this paper, we present the results of an investigation into the contrast characteristics of images of platinum particles supported on alumina. The qualitative predictions of both the phase contrast and of the diffraction contrast mechanisms of image contrast have been confirmed by experiments in which the variations in image contrast of specimen particles has been studied as the focus or specimen orientation were varied. Our results confirm that the three assumptions listed are not correct for the conditions typical in high resolution microscopy of supported metal catalysts.

Specimen Characteristics

Crucial to our considerations are the characteristics of the catalyst as a specimen for high resolution microscopy. The metal particles vary from atomic clusters (consisting of a small number of atoms, or possibly single atoms), to true microcrystallites with diameters of the order of 10 nm. The fact that the larger metal particles are crystalline, with the same face-centered cubic structure as bulk material, has been established by X-ray diffraction (*1*) and by analysis of dark-field micrographs (*12*). At the other extreme, Prestridge and Yates (*13*) have presented micrographs in which images of clusters of a few rhodium atoms have been identified. In these same micrographs, however, may be observed the strong contrast from the silica support.

The metal particles are supported on silica or alumina particles which are usually porous assemblages of irregularly shaped crystals containing defects, of which some are inherent in the crystal structure. Crushing the catalyst to a powder generally results in clumps of support particles of varying thicknesses greater than 30 nm.

The supporting material is in turn placed on microscope grids in various ways; only in the recent work of Freel (*3*) and Prestridge and Yates (*13*) have "holey carbon" support films been used, to eliminate any possibility of interference from the granular image detail observed in continuous amorphous support films [see, for example, Thon (*14*)]. From stereoscopic images we have observed that there is typically a range of elevations in the direction of the electron beam of order 100 nm, often between two apparently adjacent alumina particles. This specimen elevation, illustrated in Fig. 1, imposes a different focus condition upon various particles imaged in the same micrograph. Thus, within any one micrograph there will be a range of values of defocus (deviation from perfect focus), and within two micrographs of similar regions the range of defocus values will in general be different.

For the imaging of small atomic clusters, considerable efforts have been made to minimize the background contrast produced by the supporting film [see, for example, Ref. (*8*)]. Such films are essentially flat and only a few nanometers thick. Clearly, the typical catalyst specimen is far from ideal,

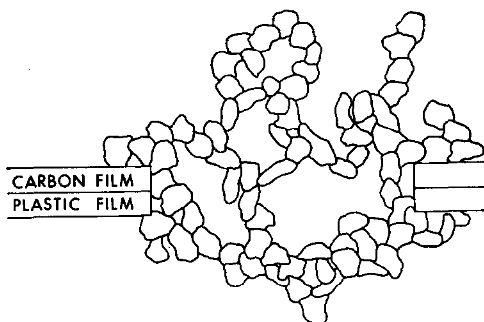

Fig. 1. Schematic cross section of typical specimen grid, showing clumping of support particles. Depth in the beam direction of order 100 nm.

in that the support imposes appreciable background contrast and holds the metal particles at different elevations.

Finally, it may be noted that the support particles, and hence the metal particles are oriented at random. Therefore any image contrast effects which are sensitive to the orientation of the electron beam may be expected to contribute to variations in contrast between otherwise identical particles.

Theory

It is clear from the characteristics of the specimens that more than one mode of image contrast formation must be considered. For the very small metal particles (clusters of atoms) the *phase contrast* mechanism will operate. However, for larger metal particles in which a definite crystalline structure has developed, the scattering process will be best described in terms of Bragg diffraction, giving rise to *diffraction contrast*. This will apply also to the essentially crystalline support particles.

We have therefore considered the implications of each of these contrast theories in what follows. There will of course be a gradation from one of these extremes to the other, but for the present purpose the intermediate case need not be considered. It was found necessary to perform fairly detailed calculations of phase contrast in order to evaluate the variation of image size with defocus. However the qualitative features of diffraction contrast are sufficiently well documented, so that additional calculations were not required.

Phase Contrast

The contrast of an image obtained in the conventional transmission electron microscope is best understood by considering the situation in the back focal plane of the objective lens, where the Fraunhofer diffraction pattern of the electron wave emerging from the specimen is formed. The objective aperture placed in this plane cuts off from the image that part of the wave corresponding to electrons which are scattered through an angle greater than that subtended by the aperture. But, in addition, the spherical aberration and the defocus of the lens have the effect of changing the phase of the wave in the back focal plane, through the "contrast transfer function," which depends also on the electron wavelength and the scattering angle. Thus, even with a large objective aperture, the microscope will not image faithfully detail smaller than 1 or 2 nm. [For recent reviews of this theory see Thon (*14*) and Hawkes (*15*).]

The way in which the phase contrast transfer function removes certain spatial frequencies from the image while changing (including reversing) the relative phases of others has been established by Thon, using amorphous thin carbon films (*14*). In order to be able to interpret the images of particles smaller than a few nanometers, the effects of lens defects must be included in suitable theoretical calculations of image contrast. This was first done by Scherzer (*11*); more recently Reimer (*10*) and Hall and Hines (*9*) have made detailed calculations of the contrast of single atoms and clusters of atoms. (The atom is considered to change the phase, but not the amplitude, of the electron wave.) Their results show that the optimum defocus values, at which maximum contrast is expected, vary with cluster size, and that for exact focus the contrast may be too low to detect. Hall and Hines (*9*) obtained through focal series of images of gold particles (on an almost structureless graphite support), which confirmed their predictions.

In order to evaluate the effects on apparent particle size of the lens defects, we have computed image profiles of atoms and atomic clusters using the formulation of Eisenhandler and Siegel (*16*). Their solution employs a real atomic scattering factor, values of which are readily available [for example, Ref. (*17*)]. This approach assumes a phase shift of $\pi/2$ upon scattering, a less accurate approach than that of Hall and Hines (*9*), who used a complex atomic scattering factor with the correct phase shift due to scattering. However, their results show that the discrepancies between the two calculations are not significant for the qualitative results in which we are interested. In these calculations, the intensity at the point (x_i, y_i) in the image

plane (scaled to unit magnification) is given by

$$|\psi(x_i, y_i)|^2 = 1 + \frac{4\pi}{\lambda}(1 - \beta^2)^{-1/2}R(x_i, y_i) \quad (1)$$

where

$\psi(x_i, y_i)$ = the wave function of the scattered electron

λ = electron wave length, set by the voltage

$(1 - \beta^2)^{-1/2}$ = relativistic correction; β is the electron velocity expressed as a fraction of the speed of light.

For a single atom, $R(x_i, y_i)$ is given by

$$R(x_i, y_i) = \int_0^{\alpha_{\max}} f_0\left(\sin\left(\frac{\alpha}{2}\right)\Big/\lambda\right)\cos\left[\frac{\pi}{2} - \frac{2\pi}{\lambda}\left(\frac{C_s\alpha^4}{4}\right) + \frac{2\pi}{\lambda}\left(\frac{\Delta f\alpha^2}{2}\right)\right] J_0\left(\frac{2\pi\alpha r_i}{\lambda}\right)\alpha d\alpha \quad (2)$$

where

α = scattering angle ($\alpha_{\max}$ is determined by the objective aperture)

f_0 = atomic scattering factor for electrons

C_s = spherical aberration constant

Δf = defocus

J_0 = zero order Bessel function

r_i = radial position in image plane from scattering center, ($r_i = (x_i^2 + y_i^2)^{1/2}$).

For multiple atom cases, the Bessel function term above is replaced by the expression

$$\sum_{n=1}^{\text{all atoms}} J_0\left(\frac{2\alpha\pi}{\lambda}((x_i + x_n)^2 + (y_i + y_n)^2)^{1/2}\right) \quad (3)$$

where x_n, y_n are the locations in the object plane of the various scattering atoms.

The term

$$\cos\left[\frac{\pi}{2} - \frac{2\pi}{\lambda}\left(\frac{C_s\alpha^4}{4}\right) + \frac{2\pi}{\lambda}\left(\frac{\Delta f\alpha^2}{2}\right)\right]$$

is the phase contrast transfer function of the lens and contains the phase changes imposed on the scattered electron wave within the lens by spherical aberration and defocus.

In order to assess the variation in image intensity for particles of different sizes, four cases were evaluated. These were arbitrarily chosen as a single atom, a three-atom planar array, a four-atom pyramidal array, and a seven-atom planar hexagonal array. For the multiple atom cases, the scattering centers (atoms) were separated by 0.275 nm, and the intensity profiles were computed along a radius which ran through a noncentral atom. Test calculations along a radius running between two noncentral atoms gave similar intensity profiles with slightly different spacings.

The calculations were performed using relativistic Hartree–Fock atomic scattering factors for gold (*17*). Values for C_s (1.6 mm) and $\alpha_{\max}$ (0.0125 radians) were chosen to be typical for a high resolution microscope at 100 kV (λ = 3.7 pm). Since a range of defocus values are expected within an image, the calculations were performed for Δf values from −200 to +400 nm in 20-nm steps.

In addition, the single atom case was evaluated over the defocus range −20 to +200 nm for four other values of $\alpha_{\max}$. These calculations were designed to test the affect of aperture size on phase contrast effects.

The R integral, Eq. (2), was iteratively evaluated, with a minimum of 200 steps to $\alpha_{\max}$, by the IMSL DRMBIU subroutine. Evaluation of ψ^2 at intervals of 0.5 nm to a total of 10 nm allowed determination of the phase contrast image profile, i.e., the image intensity as a function of spatial location in the image plane. Contrast, defined as the difference in intensity between image point and background divided by background intensity, is given by $\psi^2 - 1$.

Diffraction Contrast

For larger specimen structures the phase contrast calculation is invalid, because multiple scattering and diffraction effects become significant. Once the metal particles reach a size of 2–3 nm diameter, Bragg diffraction effects should dominate in the scattering process, and the use of standard

multibeam dynamical calculations [see, for example, Hirsch *et al.* (*18*)] is appropriate. The diffraction pattern from a single crystal consists of a series of discrete spots corresponding to diffraction from various planes in the crystal. In the back focal plane the objective aperture intercepts all except the directly transmitted beam, giving rise to bright field diffraction contrast: the variation in the intensity of the directly transmitted beam from point to point across the crystal surface. The theory then predicts a fairly sensitive dependence of image contrast on the thickness and orientation of the crystal (*18*), but a reduced sensitivity of contrast to defocus as compared with phase contrast images (*9*).

Experiment

In order to test these theoretical predictions, two series of experiments were performed. The phase contrast effects were examined by taking through focal series of each of a number of areas for both Pt/alumina and pure alumina specimens. Diffraction contrast effects were observed by imaging the same field a number of times, tilting the specimen through a known angle between each set of through focus exposures.

The micrographs were taken on a JEM100B fitted with a goniometer stage, capable of resolving the 0.34-nm spacings in graphitized carbon. All images were recorded using 100 kV accelerating voltage at a direct magnification of ×330,000, in the bright field mode.

Supported platinum catalysts were prepared by standard impregnation techniques (evaporation of salt solution followed by reduction) on Alon, an alumina that consists of small (10–30 nm) particles. This support material is particularly suitable for electron microscope studies because a minimum of irregular fracture occurs upon crushing the dried catalyst.

Catalyst samples were crushed into a fine powder and suspended in an inert solvent, then dropped onto a copper grid covered with a "holey" carbon film. The latter was prepared by condensing water droplets in a film of dissolved plastic. As the solvent evaporates and the plastic film hardens, holes are left whose size can be roughly controlled by the preparation conditions (*19*, *20*). The plastic film was then placed on an electron microscope grid and coated with a thin layer of evaporated carbon to conduct electrons and strengthen the film. When the suspended catalyst was dropped on the film, portions of the catalyst extended over the holes, so that any effects of the carbon film on the image contrast were avoided. Astigmatism was corrected at maximum magnification, and very low contamination rates were achieved through use of the standard decontamination device. Through focal series in steps of multiples of 40 nm were recorded.

The astigmatism correction was checked for selected cases, and the transfer characteristics of the lens were determined approximately from through focal series of images of thin amorphous carbon, which were analysed using a simple optical diffractometer (*14*). The optical diffraction pattern reveals which spatial frequencies are present in the image and which have been filtered out by phase cancellation (the contrast transfer function is zero for certain values of α). An example is shown in Fig. 2. The distance from the central spot is proportional to the inverse of the spatial separation and may be calibrated by imaging a known mesh. Accounting for magnification, the spatial scattering passed unfiltered for this particular pattern was calculated as 0.55, 0.67, 0.89 nm, and greater than 1.17 nm with filtering effects between these values. Alternate frequencies passed by the lens are reversed in phase relative to their original values. For this particular case, no meaningful detail less than 0.55 nm was transmitted by the lens, thus representing a limit to resolution. Elliptical rings indicate the presence of astigmatism in the objective lens which had not been completely corrected.

The objective apertures available subtended angles of approximately 0.01, 0.006, and 0.003 radians. The first of these, a 60-μm aperture, was used for most of the work reported, since the project was con-

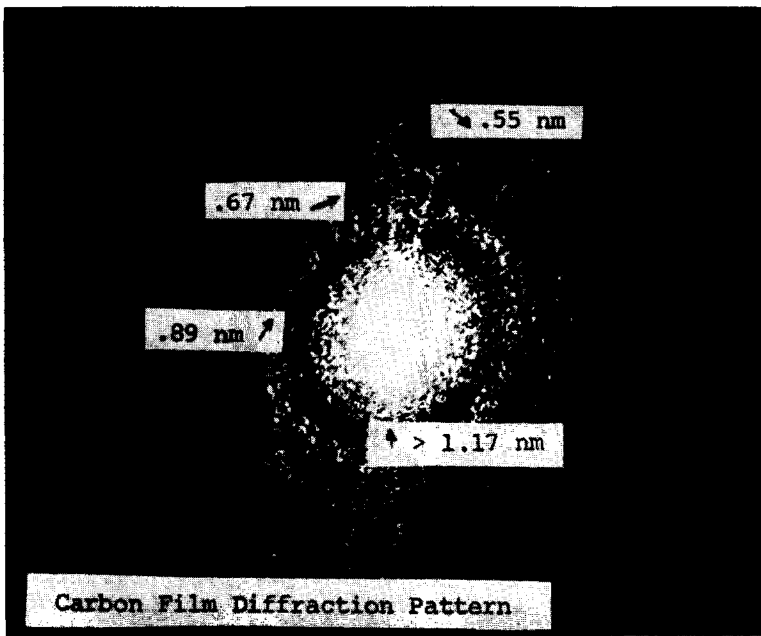

FIG. 2. Optical diffraction pattern from micrograph of thin carbon film, illustrating the elimination of certain spatial frequencies from the image.

cerned with the imaging of the smallest particles and atomic clusters. This aperture removes from the image information concerning spacings smaller than 0.37 nm, and is therefore large enough for phase contrast. On the other hand, all Bragg diffracted beams (except one) are intercepted, giving rise to diffraction contrast from the crystalline particles. The exception in our studies was the 111 reflection of γ-Al_2O_3, for which d_{111} is 0.456 nm. Lattice fringes of this spacing were often observed and were used as an internal magnification standard. The smaller apertures were used to verify the predicted effects of lower α_{max} values on image resolution.

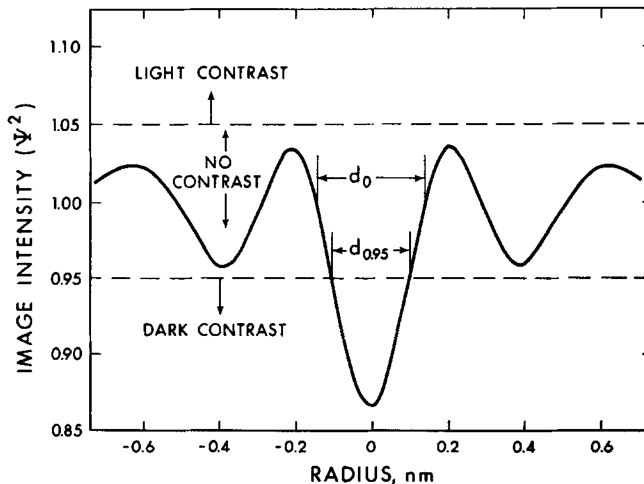

FIG. 3. Calculated image intensity profile for a single atom at a defocus of 180 nm. Dashed lines are detectability limits; two size parameters are shown.

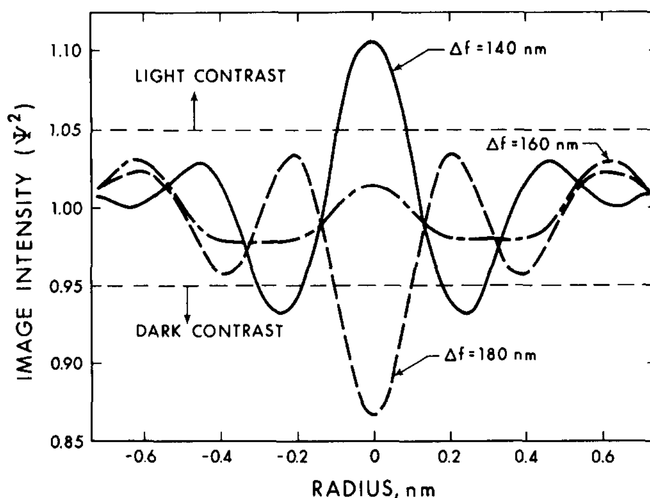

FIG. 4. Three calculated image intensity profiles for a single atom, showing the sensitivity of the image to changes in defocus.

RESULTS AND DISCUSSION

Calculated Image Profiles

Solution of the phase contrast equation generates an image intensity profile; the result for a single atom and a defocus of 180 nm is shown in Fig. 3. In order to compute detectability and size as a function of defocus, we assumed limits for distinguishable contrast, and took the width of the central peak (d_0 in Fig. 3) as the apparent size. Following Eisenhandler and Siegel (*16*), 5% light or dark maximum contrast was assumed to be necessary for detection: if the maximum intensity was between 0.95 and 1.05, the size was set to zero.

The arbitrary nature of these assumptions is evident. Other size definitions could have been chosen, such as the diameter at 5% contrast ($d_{.95}$ in Fig. 3). A different detectability limit would alter the sizes determined; under some conditions images can have bright and dark rings surrounding the central peak, with obvious complications in defining size. These and other factors would be critical if one attempted to deduce the actual size of a cluster (number of atoms) for which one would require to know the defocus value for each particle in the image. It is important to emphasize, however, that the assumption of different detectability limits or size definitions in no way affects the qualitative results of the present studies, which apply in general irrespective of the optical constants of the particular microscope being used.

Variation of Contrast and Apparent Size with Defocus

The character of an image profile is a sensitive function of focus, and can shift from light, through undetectable to dark, as shown in Fig. 4. The three profiles are for a single atom with defocus values of 140, 160, and 180 nm.

Figure 5 shows the calculated maximum image intensity of the four clusters of atoms as a function of defocus. It is evident that all four clusters will be detectable, as light or dark regions depending upon the defocus. In addition, it is evident that the range of defocus over which the arrays will appear as a region of dark contrast, the "window size," increases as the number of atoms in the cluster increases. Table 1 shows the calculated window sizes for the four cases.

In order to relate these results to micrographs of supported metal catalysts, the geometry of the specimen must be considered. Referring to Fig. 1, the specimen in the region of a hole in the grid consists of an irregular stacking of catalyst fragments, with a typical depth (measured from

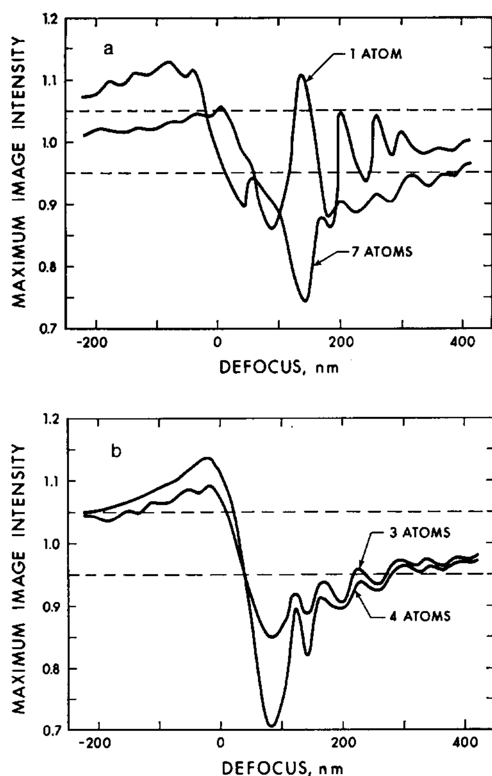

FIG. 5a and b. Calculated maximum image intensity as a function of defocus for four cases. All atom clusters will give detectable dark contrast only over a selected range of defocus values.

the image shift after tilting the specimen through a known angle) of greater than 50 nm. This depth imposes an immediate restraint on any micrograph, for the defocus over the specimen has a range equal to the depth. A large crystallite in the specimen will have dark contrast regardless of its spatial position and defocus, because of the diffraction contrast mechanism. Small metal clusters, however, have a contrast which is extremely sensitive to the defocus, and thus only some regions of the specimen may be so situated as to provide dark phase contrast for these small particles.

TABLE 1
THEORETICAL DEFOCUS WINDOWS FOR DARK CONTRAST FOR VARIOUS ATOMIC CLUSTERS
(C_s = 1.6 mm, λ = 3.7 pm)

Case	Windows
1 atom	60–120; 150–195; 235–250
3 atoms	45–215; 240–275
4 atoms	40–280
7 atoms	10–390

Calculated apparent size of metal clusters is also a sensitive function of the defocus, as shown for the three- and seven-atom cases in Fig. 6. Even in the region where clusters give dark contrast, the sharpness and diameter of their images varies strongly with defocus. Thus, again returning to an actual catalyst specimen, identical small metal particles at different elevations in the specimen would be expected to have varying image sizes, because the variation in defocus for these particles is equal to their differences in elevation in the specimen. Similarly, identical particles imaged in different micrographs would in general appear of different size because of differences in defocus.

An extreme case of the deviation in calculated image appearance with defocus for the four atom case is shown in Fig. 7. A 60-nm change in defocus changes the image from a dark region of 0.8 nm apparent diameter, to a ringed dark–light pattern, with an apparent size for the inner dark region of 0.4 nm.

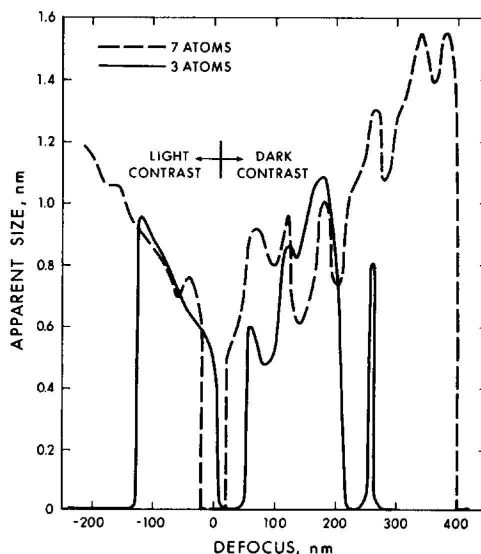

FIG. 6. Calculated apparent image size as a function of defocus. The size of the image is not a simple function of the size of the specimen particle.

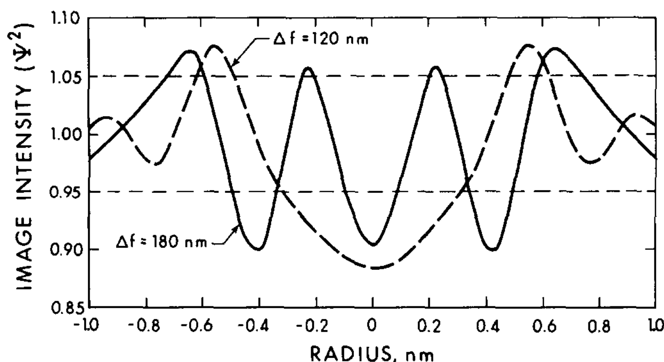

FIG. 7. Two calculated image intensity profiles for the four atom case, showing the sensitivity of apparent image size to defocus.

Analysis of a series of micrographs of a 4.76% Pt on Alon catalyst confirms that for small contrast regions detectability and apparent size are a sensitive function of the defocus. Figure 8 shows micrographs of identical areas of catalyst at various values of defocus. (Reproduction may have reduced the quality of the micrograph; prints are available on request from the authors.) Between the two micrographs shown in Fig. 8a, there is a difference in defocus of 80 nm. Regions "*a*" and "*d*" show the distortion of apparent shape effected by the defocus change. The dark region *a* appears to resolve into two crystallites in the right hand micrograph, while the shape of particle *d* is substantially altered. The region of contrast above *c* is enhanced in the right hand picture. Regions *b*, *e*, *f*, and *g* show the fine contrast detail which alters with defocus; in each region particular subnanometer structure is apparent or highlighted in one micrograph, but not in the other. Similar effects are observable near regions *a*, *b*, and *c* in Fig. 8b, for which the change in focus is 40 nm.

The fact that it is not possible to decide from such micrographs whether this fine contrast arises from platinum particles or from the substrate is discussed later.

Measurements of apparent image size were made for a number of particles in each micrograph of a through focal series. The results are plotted in Fig. 9 for three separate fields of view, and it is evident that "window sizes" are smaller and relative fluctuations in apparent sizes greater, for the smaller contrast regions. These results confirm the qualitative predictions made on the basis of the phase contrast calculations (see Fig. 5 and Table 1).

These results make it quite clear that the number of particles which will be detected in a standard size analysis will depend upon the average defocus value of the micrograph as a whole, and on the particular defocus range existing within the micrograph. Identical small particles at different elevations in the specimen will have different apparent sizes, or may not be detectable simultaneously. The observed variation in apparent size of up to 1 nm imposes an uncertainty on measured sizes, which implies that for analysis of size distribution, division of sizes into classes which differ by less than 1 nm is not warranted.

As aperture size is reduced, calculations indicate that the variation in image intensity and apparent size decreases, but at the expense of contrast and size information (*9*). This is shown in Table 2, where for the single atom case the maximum image contrast and apparent size are shown over a defocus range for varying apertures, and hence varying values of α_{max}. For the α_{max} value of 0.005 radians, no contrast above 5%, light or dark, is realized in this defocus range, while for a very small aperture giving an α_{max} of 0.00125 radians, even 0.1% contrast is not achieved. As the aperture is decreased, the image size increases, until for the smallest aperture, the atom, if de-

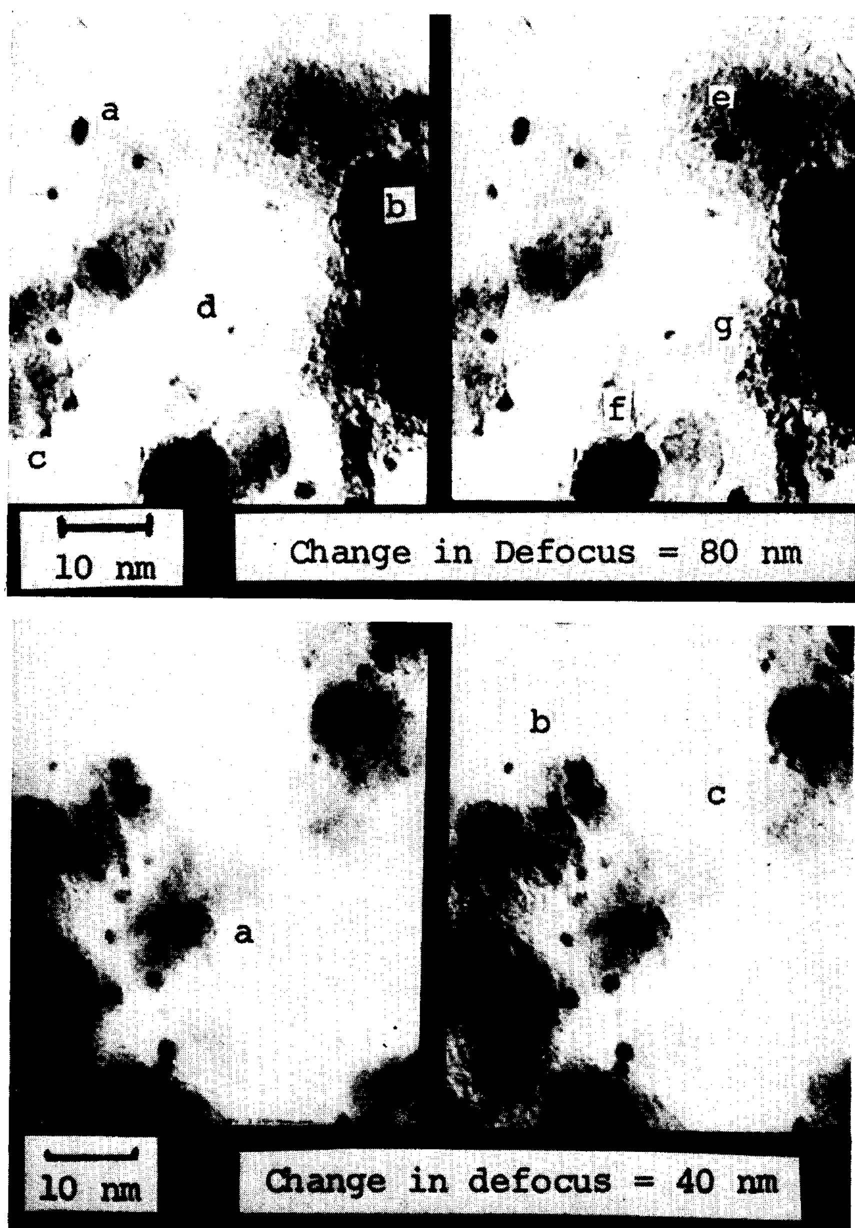

FIG. 8. (top and bottom) Micrographs of a Pt/Al_2O_3 catalyst showing the effect of defocus change on image contrast.

tected, would appear to be greater than 2 nm in size. Thus variations in image appearance with defocus are reduced by smaller apertures, but at the cost of image intensity and size definition of the image.

Through focal series of images were recorded of the same specimen area for apertures subtending angles of 0.01, 0.006, and 0.003 radians. The predicted loss of resolution was observed with some very small regions of dark contrast, clearly resolved in the image recorded with an α_{max} of 0.01, but being progressively washed out through lower contrast and increased size as the aperture size was reduced.

It may be noted that if one is not concerned with detection of particles less than about 2 nm, the use of smaller apertures is

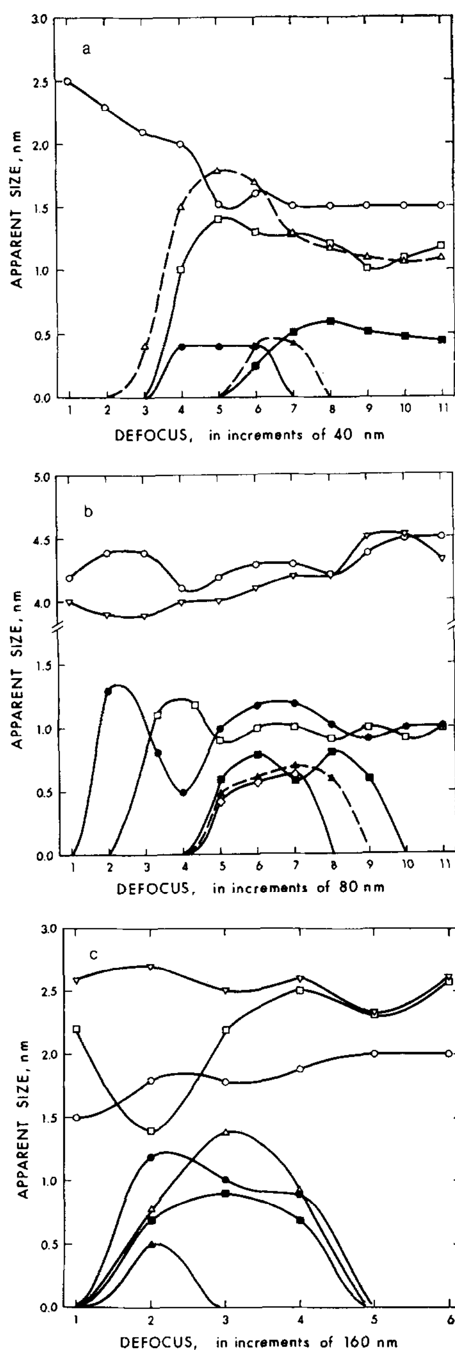

FIG. 9a, b and c. Variation of measured particle size with defocus for three through focus series of micrographs of a Pt/Al_2O_3 catalyst. Zero values mean that the particle was not detected.

probably advantageous. The variation of intensity with defocus is reduced for smaller apertures and the diffraction contrast of particles is greater, although we still observed some variation of apparent size with defocus.

The Effect of Tilt on Contrast

The sensitivity of the contrast of both metal microcrystallites and support particles to the orientation of the electron beam was investigated using the high resolution tilting holder. Micrographs of a specimen being tilted differ not only in angle of orientation to the electron beam, but also differ slightly in the defocus condition. This latter occurs because during tilting the specimen shifts physically in the object plane, and an exact restoration of the previous defocus value is impossible. However variations in regions of contrast greater than 2–3 nm can be attributed to orientation effects, since phase contrast effects become minimal at these sizes.

The micrographs in Fig. 10 show identical specimen areas with a variation in tilt angle. In Fig. 10a, a tilt change of 15° significantly alters the appearance of the metal particles. The particle in region *a* disappears in the right hand micrograph, while a third crystallite in region *c* is more clearly evident in the right hand micrograph. The two particles in region *b* appear as one in the right hand micrograph possibly due to superposition. The sensitivity of support contrast to orientation is evident to the right of region *c*. Similarly, in Fig. 10b, several contrast alterations are evident with a tilt change of 7°. The relative contrast of the two particles in region *a* changes, revealing the sensitivity of contrast to orientation. A contrast region to the right of region *c* is not detected in the right hand micrograph. In regions *b* and *d*, the background contrast is reduced substantially as a result of tilt; in region *b* this results in highlighting of a particle virtually obscured in the left hand photograph.

The simultaneous variations in support and metal particle image contrast again raises questions about the reliability of single micrograph particle size distribution analysis. The variation in orientation leads to a change in apparent contrast of a particle. For larger particles, this contrast change would not be sufficient to prevent

TABLE 2

Calculated Image Intensity and Apparent Size Over a Range of Defocus and Apertures

Aperture (μm):	40		32		16		8		4	
α_{max} (radians):	0.0125		0.0100		0.0050		0.0025		0.00125	
Defocus (nm)	I_{max}[a]	d_0[b]	I_{max}	d_0	I_{max}	d_0	I_{max}	d_0	I_{max}	d_0
−20	1.039	0.56	1.051	0.56	1.017	0.70	1.001	1.44	1.000	>2.0
0	1.053	0.50	1.036	0.52	1.007	0.66	1.001	1.30	1.000	>2.0
20	1.037	0.40	1.035	0.40	0.996	0.86	0.999	1.46	1.000	>2.0
40	1.005	0.14	1.023	0.22	0.986	0.76	0.999	1.45	1.000	>2.0
60	0.950	0.56	0.943	0.56	0.976	0.75	0.998	1.45	1.000	>2.0
80	0.860	0.43	0.847	0.45	0.969	0.75	0.997	1.45	1.000	>2.0
100	0.868	0.46	0.867	0.48	0.964	0.76	0.997	1.45	1.000	>2.0
120	0.954	0.80	0.993	0.74	0.961	0.78	0.996	1.45	1.000	>2.0
140	1.105	0.26	1.060	0.26	0.962	0.80	0.995	1.45	1.000	>2.0
160	1.014	0.18	1.003	0.12	0.965	0.86	0.995	1.44	1.000	>2.0
180	0.865	0.30	0.944	0.40	0.970	0.92	0.994	1.44	1.000	>2.0
200	1.049	0.20	0.972	1.20	0.977	1.04	0.994	1.45	1.000	>2.0

[a] Calculated so that background intensity is 1.0.

[b] In nanometers.

detection, but for smaller particles the orientation clearly can prevent their being included in a particle count. Since a typical supported metal catalyst contains particles at all orientations, the danger of miscount is evident.

Contrast Structure in the Support Material

An additional concern in assessing the accuracy of particle size distribution analysis is the distinguishability of small crystallite images from the contrast inherent in the support. Typical support materials, such as alumina or silica, have a highly irregular structure leading to high surface areas. This irregularity is a desired feature for catalysts, allowing a large gas–solid interface and a high dispersion of metal. Diffraction evidence from alumina support materials confirms a fine polycrystalline structure.

The polycrystalline irregular structure leads to considerable contrast variation in the micrograph of alumina itself. Such contrast structure is on a small (down to 0.5 nm) scale, and is particularly evident in regions of crystal overlap.

Figure 11 demonstrates this effect. The left-hand micrograph shows two regions of catalyst at different elevation. In the right-hand micrograph, the grid has been tilted through 25° so that these regions now overlap. Considerable contrast structure is evident along the line of overlap which does not arise from the presence of metal crystallites detectable in the left-hand micrograph. This contrast structure is indistinguishable in a standard micrograph from that which is generated by small crystallites. Examination of micrographs of pure Alon, with no platinum added, show this fine contrast structure, again particularly in overlap and boundary regions; Fig. 12 illustrates this.

The inherent support contrast structure limits the lower size limit to which particle size analysis may be extended. Even where microscope resolution is better than 1 nm, distinction of metal particle from support contrast in this size range is virtually impossible in a single bright field micrograph.

Conclusions

A number of conclusions concerning the determination of particle size distribution of supported metal catalysts from electron micrographs emerge from the work reported in this paper.

1. For metal particles below about 2 nm in diameter:

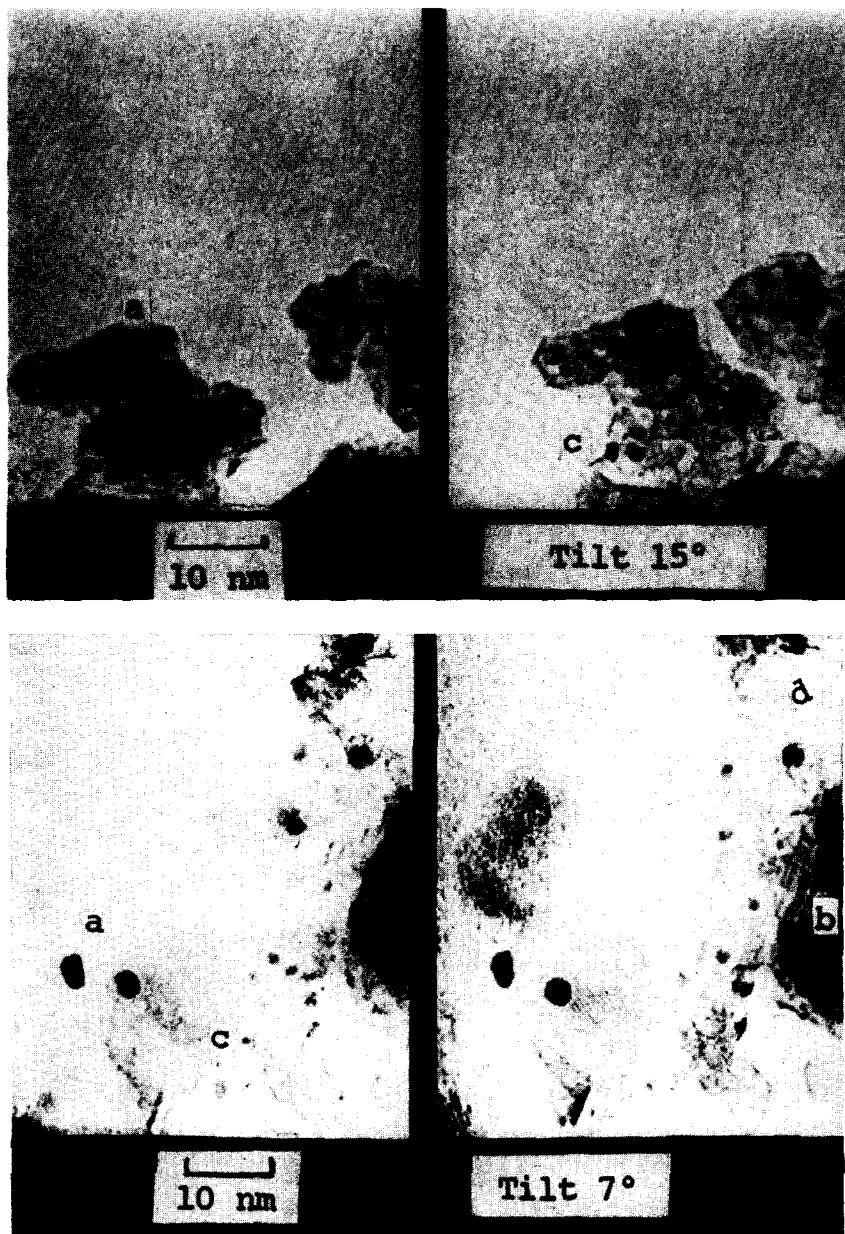

FIG. 10. (top and bottom) Micrographs of a Pt/Al_2O_3 catalyst showing the effect of tilt on image contrast.

a. Because of the phase contrast mechanism, detection is a sensitive function of the defocus and hence of the spatial elevation in the specimen. As metal clusters get smaller, the defocus range over which they are detectable as a region of dark contrast decreases; b. Apparent size is a sensitive function of defocus, since the microscope "filters" certain spatial frequencies and thus distorts the images. Thus identical clusters will have apparent images which vary with their spatial elevation in the specimen, within a single field of view. Identical particles in separate micrographs could appear to have differing sizes because of different settings of the objective focus.

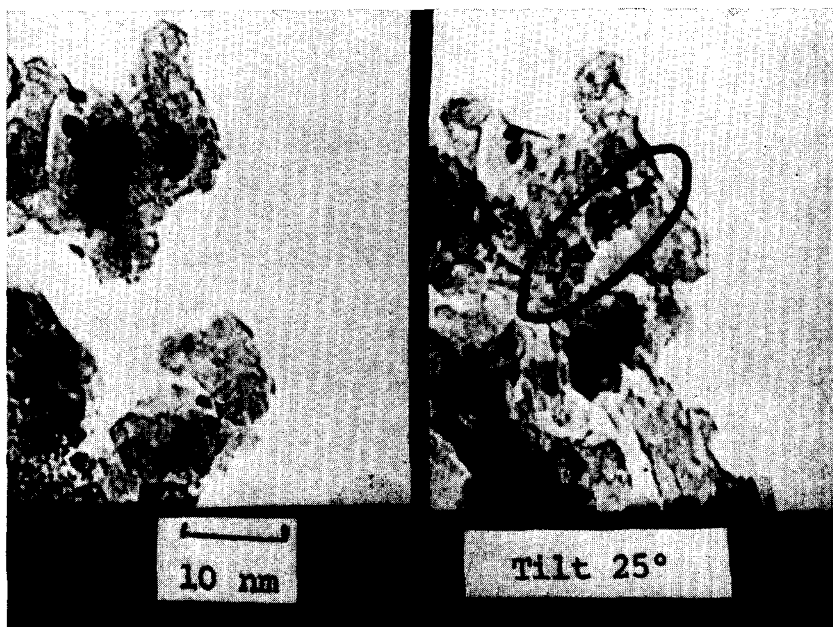

FIG. 11. Micrographs of a Pt/Al_2O_3 catalyst showing the effect of tilt on contrast. Note fine contrast structure along overlap region in the right hand micrograph.

Further, variation in apparent particle size of up to 1 nm suggests this value as the lowest meaningful division of diameters in a particle size distribution;

c. An inherent contrast is generated by the use of irregular polycrystalline supports. Particularly for metal particle images below 1 nm, distinction of particle images from background

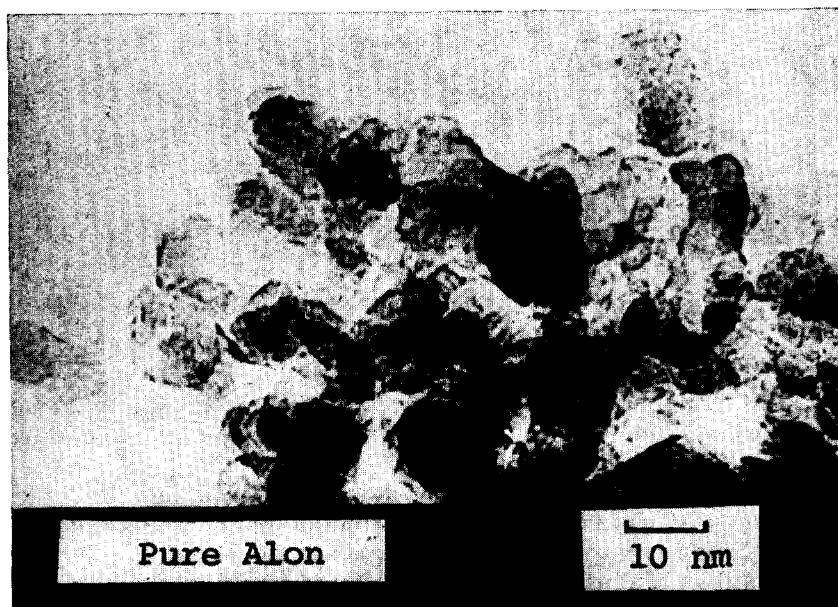

FIG. 12. Micrograph of pure Al_2O_3 ("Alon") specimen showing the contrast inherent in the support.

contrast is virtually impossible within a single bright field micrograph.
2. For large metal particles, identical crystallites can have markedly different contrast due to different orientation to the electron beam.
3. For all sizes of metal particle, the effects of overlap, and the orientation sensitivity of the contrast of the support material, can seriously affect size analysis. Certain combinations of particle/support orientation make the particle undetectable.

It is evident that these conclusions are incompatible with the assumptions implicit in some applications of particle size distribution analysis of supported metal catalysts. Clear evidence of the detection of a crystallite of a given size does not imply that all crystallites of that size and larger are being detected, because of contrast window and orientation factors. Small image sizes cannot in general be directly correlated to the particle size in the specimen, preventing computation of a meaningful average size for catalysts containing small metal particles. Analysis of such catalysts is further complicated by the difficulty of distinguishing metal contrast from inherent support contrast.

These conclusions draw into question the extension of particle size analysis into the subnanometer range; they further imply that analysis of micrographs cannot currently provide a definitive test of adsorption stoichiometries for small crystallites (*6*). As a general rule, we would argue that particle size distributions become increasingly unreliable as the size of particles counted extends below 2.5 nm. While micrographs can give evidence of smaller particles, detection and accurate identification of all particles of a size below 2.5 nm is extremely unlikely.

It should be emphasized, however, that the present studies have been concerned only with the use of conventional high resolution transmission electron microscopes, using standard bright field imaging. There are a number of other imaging techniques which may prove more suitable after similar detailed evaluation. We are currently evaluating the use of dark-field images, which have proved valuable for the detection of single heavy atoms (*21*) and for relatively large supported metal particles (*22*). A more promising possibility in the long term may well be the use of scanning transmission instruments of the type developed by Crewe and his colleagues (*23*), which permit a range of new contrast mechanisms to be applied.

ACKNOWLEDGMENTS

The authors express their appreciation to the National Research Council of Canada for the financial support provided for this study. One of us (P.C.F.) also gratefully acknowledges the support of the International Nickel Company of Canada, Ltd., through an International Nickel Research Fellowship. Valuable discussions with colleagues, in particular, Dr. S. S. Sheinin, are acknowledged with thanks.

REFERENCES

1. ADAMS, C. R., BENESI, H. A., CURTIS, R. M., AND MEISENHEIMER, R. G., *J. Catal.* **1**, 336 (1962).
2. CORMACK, D., AND MOSS, R. L., *J. Catal.* **13**, 1 (1969).
3. FREEL, J., *J. Catal.* **25**, 139 (1972).
4. MOSS, R. L., *Platinum Metal Rev.* **11**, 141 (1967).
5. POPE, D., SMITH, W. L., EASTLAKE, M. J., AND MOSS, R. L., *J. Catal.* **22**, 72 (1971).
6. WILSON, G. R., AND HALL, W. K., *J. Catal.* **17**, 190 (1970).
7. WILSON, G. R., AND HALL, W. K., *J. Catal.* **24**, 306 (1972).
8. FORMANEK, H., MUELLER, M., HAHN, M. H., AND KOLLER, T., *Naturwissenschaften* **58**, 339 (1971).
9. HALL, C. R., AND HINES, R. L., *Phil. Mag.* **21**, 1175 (1970).
10. REIMER, L., *Z. Naturforsch. A* **24**, 377 (1969).
11. SCHERZER, O., *J. Appl. Phys.* **20**, 20 (1949).
12. AVERY, N. R., AND SANDERS, J. V., *J. Catal.* **18**, 129 (1970).
13. PRESTRIDGE, E. B., AND YATES, D. J. C., *Nature (London)* **234**, 345 (1971).
14. THON, F., *in* "Electron Microscopy in Material Science" (V. Valdre and A. Zichichi, Eds.), p. 570. Academic Press, New York, 1971.
15. HAWKES, P. W., "Electron Optics and Electron Microscopy." Taylor and Francis, London, 1972.

16. EISENHANDLER, C. B., AND SIEGEL, B. M., *J. Appl. Phys.* **37**, 4, 1613 (1966).

17. DOYLE, P. A., AND TURNER, P. S., *Acta Crystallogr. A* **24**, 390 (1968).

18. HIRSCH, P. B., HOWIE, A., NICHOLSON, R. B., PASHLEY, D. W., AND WHELAN, M. J., "Electron Microscopy of Thin Crystals." Butterworth, London, 1965.

19. FUKAMI, A., AND ADACHI, K., *J. Electronmicrosc.* **14**, 112 (1965).

20. FUKAMI, A., ADACHI, K., AND KATOK, M., *J. Electronmicrosc.* **21**, 19 (1972).

21. HASHIMOTO, H., KUMAO, A., HINO, K., YOTSUMOTO, H., AND ONO, A., *Jap. J. Appl. Phys.* **10**, 1115 (1971).

22. FORNWALT, D. E., AND KINOSHITA, K., *Micron* **4**, 99 (1973).

23. CREWE, A. V., AND WALL, J., *Optik* **30**, 461 (1970).